Available online at www.sciencedirect.com
SCIENCE DIRECT
Scripta Materialia 54 (2006) 1379–1383
Scripta MATERIALIA
www.actamat-journals.com

Influence of relative density on the architecture and mechanical behaviour of a steel metallic wool

J.P. Masse [a,*], L. Salvo [a], D. Rodney [a], Y. Bréchet [a], O. Bouaziz [b]

[a] *Institut National Polytechnique de Grenoble, ENSPG, GPM2, BP 46, 38402 Saint-Martin d'Hères Cedex, France*
[b] *Arcelor Research, Voie Romaine, BP 30320, 57283 Maizières Les Metz, France*

Received 13 July 2005; received in revised form 1 September 2005; accepted 28 November 2005
Available online 18 January 2006

Abstract

This aim of this paper is to present the influence of density on the mechanical behaviour of steel metallic wool. The stress–density curves follow a power–law relationship in accordance with some models. The exponent of the power–law varies from 3 to 5 with the density and this evolution is correlated with the architecture of the metallic wool.

Keywords: Metallic wool; Entangled material; Mechanical properties; Structural characterisation; X-ray micro-tomography

1. Introduction

Entangled materials can be natural materials (sheep's wool, cotton) or artificial ones (steel wool, glass wool, felts). They find applications in thermal insulation, mechanical reinforcement and filtration. These kinds of materials are close to cellular materials, with regard to their low density and discrete architecture. The state of knowledge about metal foams is well developed, from both experimental and modelling viewpoints [1,2]. Comparatively entangled materials have been much less investigated. Metallic wools, sintered in order to create permanent cross-links between the fibres, have been considered [3,4]. In the case of non-sintered entangled materials, compression experiments have been performed on several type of entangled materials, natural (such as animal wool and human hair), and synthetic (such as carbon nanotubes [5]). Models to understand the mechanical behaviour of non-bonded fibrous material have been proposed [6–8]; essentially based on dimension analysis, they established a power–law relationship between stress and fibre volume fraction during compression testing. Recently, this scaling law has been confirmed by discrete three-dimensional (3D) simulations [9]. Other analytical models for isotropic bonded arrays have also been proposed [10].

The purpose of the present work is to study the mechanical behaviour of a non-sintered steel wool with a very low volume fraction of fibre (less than 2%). We will focus on the influence of the initial fibre volume fraction on the Young's modulus and the whole stress–strain curve during compression tests and experiments will be compared to the existing models.

1.1. Material

Fig. 1(a) shows an example of the metallic wool considered here, along with the notation for the principal axis used throughout this article. Note in particular that the direction x_2 is the rolling direction. The metallic wool was provided in the form of a strip (5 mm in thickness and 27 cm wide) and is made of stainless steel AISI 434 fibres. The cohesion of the material is only due to the fibres entanglement. The global surface mass of the wool is 1 kg/m^2, which corresponds to an average fibre volume fraction

* Corresponding author.
E-mail address: jeanphilippe.masse@gpm2.inpg.fr (J.P. Masse).

1359-6462/$ - see front matter
doi:10.1016/j.scriptamat.2005.11.075

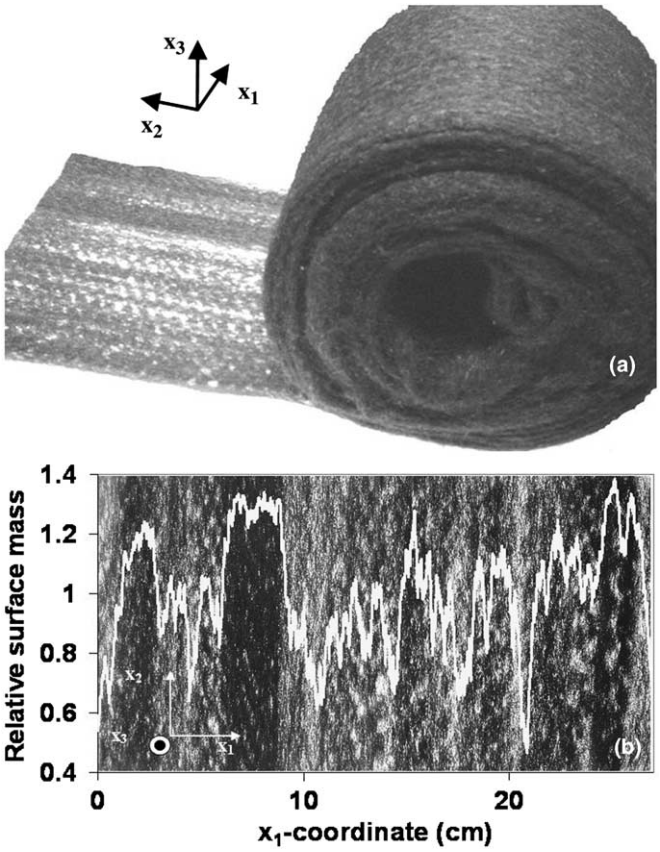

Fig. 1. View of the metallic wool: (a) macroscopic view with principal directions and (b) centimetric view with the variation of the relative surface mass along the x_1 direction (white curve) superimposed. (The band is 10 cm in height along the x_2 direction.)

of 2% approximately. As shown in Fig. 1(a), the material is clearly anisotropic and reveals parallel bands of homogeneous density in the x_2 direction.

1.2. Structural characterization

First we characterised the fibres by extracting over 300 individual fibres from the wool and measuring their characteristics. Their mean free length was about 5 mm. The sections of the fibres were analysed using optical microscopy and two-dimensional (2D) image analysis on individual fibres cut and placed vertically in a mould and impregnated with resin: the area was measured on both sides of the mould after polishing and a mean area of 525 μm^2 was found, which gives an equivalent diameter of 13 μm. This leads to an aspect ratio of about 400.

Second the local density variation along the x_1 direction was quantified using 2D image analysis. An image of a 27 cm × 10 cm band was taken and the grey level was calibrated with the local surface mass: a purely white region is associated with a surface mass of 0 kg/m^2 and the mean grey level of the image associated with the surface mass of the band 1 kg/m^2. A linear correlation was then applied. The local surface mass variation along x_1 was obtained by averaging the grey level along a column of three pixels wide and displaced along x_1. Fig. 1(b) presents the results normalised by the surface mass of the band. The relative surface mass ranges from 0.6 to 1.4 and thus it confirms the existence of bands with homogeneous surface mass along x_2. This allows the extraction of samples (30 mm × 30 mm) of various but homogeneous surface mass from the same band for the compression experiments.

Finally, two homogeneous samples with different surface masses (0.7 and 1.3 kg/m^2) were analysed in a scanning electron microscope (SEM), in order to study the influence of the surface mass on the architecture of the metallic wool (Fig. 2(a) and (b)). Qualitatively, one can see that the structures of the fibres are more aligned in the x_2 direction for the high surface mass sample in comparison with the low surface mass sample (Fig. 2(a) and (b)). Thus in order to quantify these observations we used X-ray micro-tomography to get 3D images of samples with various surface mass taken in homogeneous bands. X-ray micro-tomography experiments were performed at ESRF (European synchrotron radiation facility) on ID 15 line; 900 projections were taken over 180° degrees and recorded with a 1024 × 1024 FRELON CCD camera, with a pixel size of 1.46 μm. This resolution is required since the mean diameter of the fibres is 13 μm; therefore, the size of the explored sample in X-ray

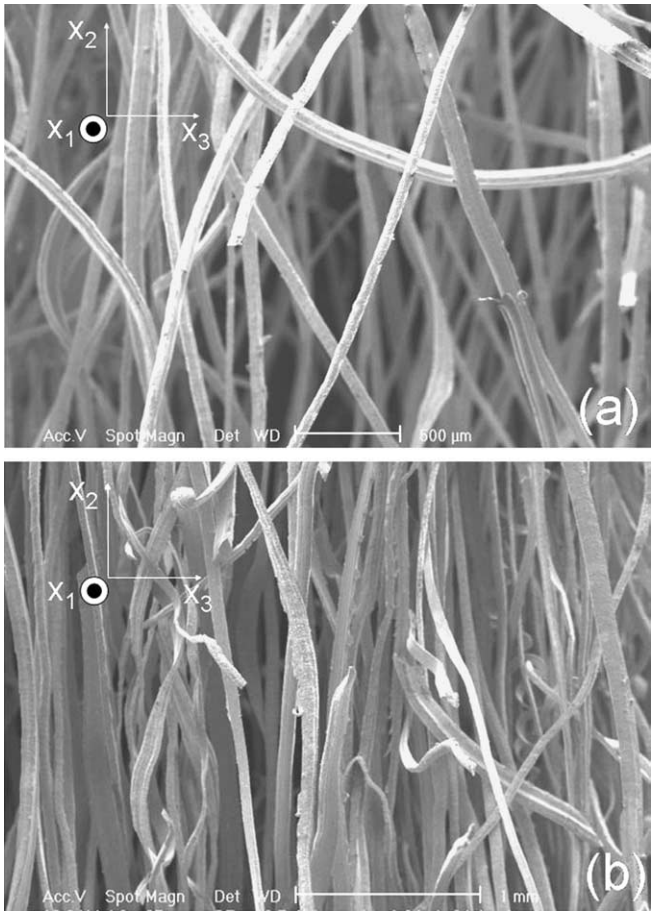

Fig. 2. SEM view of the metallic wools in the thickness in a band of surface mass: (a) 0.7 kg/m^2 and (b) 1.3 kg/m^2.

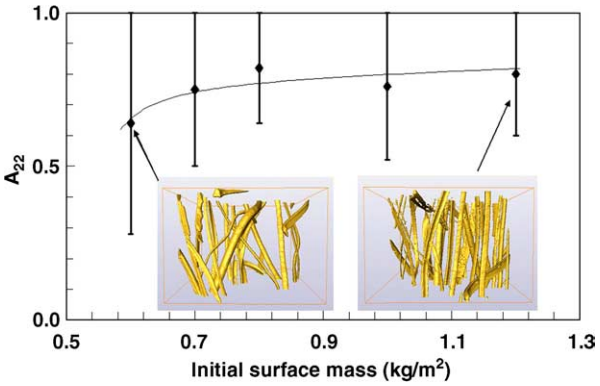

Fig. 3. Influence of surface mass on the component A_{22} of the orientation tensor of the fibres. 3D renderings of two corresponding samples obtained from X-ray micro-tomography experiments are also shown (height of sample ~1 mm).

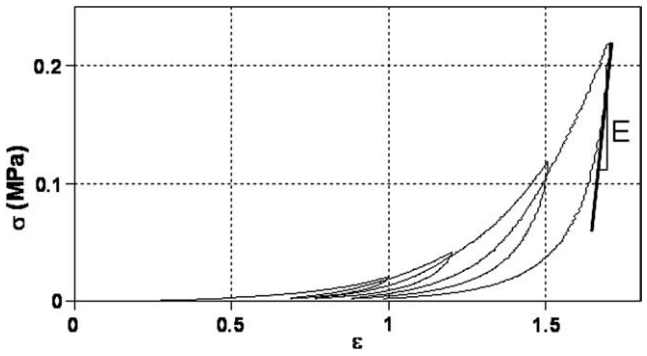

Fig. 4. Typical curve nominal stress versus true strain for compression with unloads.

tomography is of the order of 1 mm in each direction. At this scale the apparent tortuosity shown in Fig. 2(a) is negligible. Fibres are separated thanks to 3D erosion morphological operation and their principal direction obtained using their inertia matrix. Using the axis vector $\vec{n}$ of the fibres, we determined the average orientation tensor of the fibres defined as $[A] = \frac{1}{N}\sum \vec{n} \otimes \vec{n}$, where N is the number of fibres. For all the samples the major term is A_{22}, which indicates the alignment of the fibres in the x_2 direction. The others are negligible, except A_{23}, which decreases with surface mass, indicating that the fibres are less aligned in-plane (x_2, x_3), which was observed in SEM (Fig. 2(a) and (b)). Fig. 3 shows the influence of surface mass on A_{22} and the 3D rendering obtained from X-ray tomography data: at low surface mass $A_{22} = 0.6$ while it can reach up to 0.8 at large surface mass. This is in accordance with SEM observations and can be explained since for low surface mass, the fibres have more degree of freedom to entangle. Furthermore it seems that the surface mass influence on A_{22} is non-linear and a saturation value of 0.8 is obtained, at least in the surface mass range investigated in this study. The higher the surface mass, the lower is the scatter in A_{22}, which is also an indication of the fibre alignment in the x_2 direction.

1.3. Mechanical characterization

The metallic wool was characterized by uniaxial compression tests in the direction x_3. Square samples (30 mm × 30 mm) of homogeneous surface mass, ranging from 0.6 to 1.4 kg/m^2, were extracted in the bands shown in Fig. 2. The samples are compressed between two plates without any lubrication using a 2 kN cell load and a linear variable displacement transducer (LVDT) to measure the displacement. The LVDT resolution is 0.1% on a total displacement of 20 mm, which means a 20 μm resolution on displacement. All tests were conducted at a constant strain rate of 0.03 s^{-1}. A typical curve is presented in Fig. 4, in which the sample undergoes unloading from which the Young's modulus, E, is obtained for a given strain as indicated in Fig. 4. For clarity only four unloadings are shown but in practice, we performed 60 unloadings during the compression experiments to derive the Young's modulus versus the strain. A hysteresis is observed during the loading/unloading cycles, which is often reported in the literature [3,4] and may be attributed either to the friction between the fibres and/or irreversible fibre rearrangements. The true strain is converted into a density using the relationship:

$$\rho = \rho_0 \exp(-\varepsilon) \text{ with } \varepsilon = \ln\left(\frac{h}{h_0}\right)$$

Making use of these relations, the stress–strain curves are redrawn as stress–density curves on a log–log scale (as shown in Fig. 5(a)), in order to compare our experimental results with the analytical models proposed by Van Wyk [6] and Toll [7]. In these models micromechanical theory is derived, based on contact point statistics and bending of fibres using beam theory. The aspect ratio of 400 in our material makes such a hypothesis reasonable. The latter models yield the following relationship between the stress σ and the density ρ of random wools that deform by bending between fibre contact points:

$$\sigma = kE_f(\rho^n - \rho_c^n)$$

The factor k is a single adjustable parameter of the model and accounts for orientation distribution and degree of crimp, as well as the constraints and loading direction of the fibre segments. E_f is the fibre's Young's modulus. The exponent n, which is the slope of the stress–density curve on a log–log scale, is a function of the wool structure: $n = 3$ for a random 3D structure [6] and $n = 5$ for random 2D plane structure [7]. Finally, ρ_c is the threshold volume fraction (also called the packing density) below which the wool has no mechanical response. Fig. 5(a) shows three loading curves obtained from samples with different initial surface masses. These curves confirm the existence of threshold densities below which the samples have no mechanical response. Beyond these, the linearity of the curves in this log–log scale confirms the power–law relation between the stress and the density. The exponents n are

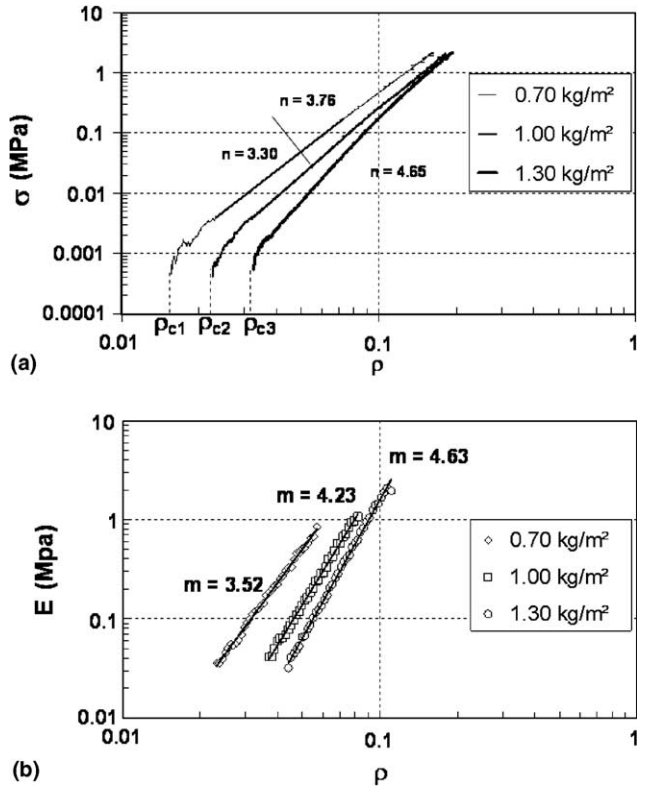

Fig. 5. Mechanical curves: (a) stress–density and (b) Young's modulus–density (obtained from unloading experiments) on a log–log scale for three different initial surface masses.

noted on the figure. From these loading curves, we can derive a tangent modulus E. From previous equation this modulus $E_{\tan g} = \frac{d\sigma}{d\varepsilon} = nkE_f\rho^n$ is characterised by the same exponent n as the stress.

Thanks to the unloading experiments that were carried out, it is also possible to calculate the Young's modulus, E, and plot it (in Fig. 5(b)) as a function of the density rather than strain, on a log–log scale. Fig. 5(b) shows clearly that for a given initial surface mass the Young's modulus is a linear function of the density on the log–log scale and thus the Young's modulus has also a power–law relation with density: $E = \beta\rho^m$.

Fig. 5(a) and (b) show clearly that the exponent n and m are functions of the initial surface mass of the sample and increase as the surface mass increases. The exponents are larger than one, which is characteristic of entangled materials, in which the number of fibre to fibre contacts evolves during compression This feature is indeed taken into account in the model [6,7]. By contrast the model developed for isotropic bonded fibre array [10] predicts an exponent of 1. In addition, as shown in Fig. 5(a), the higher the surface mass, the larger is the threshold density. Fig. 6 presents the evolution of the exponents n and m with the surface mass. Firstly, it can be noticed that n and m present the same trend, which means that both the tangent modulus and the unloading modulus present identical evolution with the surface mass. The reason for such a comparable variation is not clear and will need further study to be

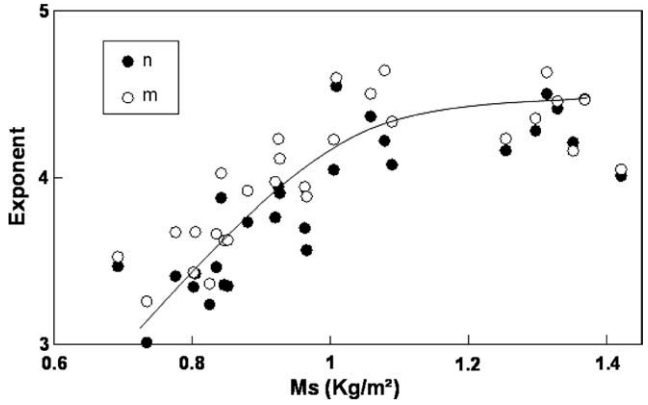

Fig. 6. Variation of the two exponents n and m with the initial surface mass.

understood. Secondly, the exponent (n or m) starts at low surface mass from a value of 3.5 increases linearly up to 4.5 and seems to stabilize to this value for a surface mass larger than 1.1 kg/m^2. These values can be compared to those derived by Van Wyk and Toll [6,7] for two specific architectures: a 3D random structure gives an exponent of 3 and a 2D random plane structure an exponent of 5, whatever the surface mass. It is not surprising to find values of exponents that are different from the two extreme cases since the architecture analysis clearly shows that whatever the surface mass, the metallic wool can not be considered as a 3D random or even a 2D random fibre network. The fact that the exponent lies in between these two extreme case indicates that the structure of the wool present an architecture that is in between the 2D random and the 3D random. The variation can furthermore be correlated to the change of structure of the wool with the surface mass that we observed and quantified. Indeed the component A_{22} of the orientation tensor, which seems to be a relevant parameter to characterise the structure evolution and the alignment of the fibre in the x_2 direction, increases with the initial surface mass (see Fig. 3). One can see in Fig. 5(a) (extrapolating to the origin) that k decreases as the surface mass increases (i.e., when the architecture becomes "more 2D"), but, due to the phenomenological definition of k, the physical interpretation of this experimental fact is unclear.

2. Conclusion

We studied the mechanical behaviour of metallic entangled materials with surface mass ranging from 0.6 kg/m^2 to 1.4 kg/m^2. The main results are:

- The metallic wool is heterogeneous in surface mass in the x_1 direction (perpendicular to the rolling direction). Bands of homogeneous surface mass ranging from 0.6 kg/m^2 to 1.4 kg/m^2 can be obtained.
- The orientation tensor of homogeneous density samples has been determined from X-ray tomography data and it is clear that the higher the surface mass, the more

the fibres are aligned in the rolling direction: the component A_{22} of this tensor is a relevant parameter to characterise the architecture.
- The stress–density curve is well fitted by a power law model in the whole surface mass range.
- The exponent of the stress–density power law varies with surface mass, increasing from 3.5 to 4.5 and reaching a "plateau" at a surface mass of 1 kg/m^2.
- The variation of the exponent with the surface mass is correlated with the structure variation: it seems that orientation tensor and especially the A_{22} component.
- The variation of the Young's modulus, obtained from unloading experiments, with the density is also described by a power law. The variation of this exponent with the surface mass is the same as the variation of the exponent that relates stress to density. This basically means that the influence of the density is the same for the tangent and the unloading moduli.

Acknowledgements

The authors would like to thank Arcelor Research for funding this study. They acknowledge stimulating discussions with Drs. R. Dendievel and M. Fivel. They would like also to thank M. Di Michiel and ID15 line of ESRF for X-ray tomography experiments.

References

[1] Ashby MF, Evans AG, Fleck NA, Gibson LJ, Hutchinson JW, Wadley HNG. Metal Foams : A design guide. Boston (MA): Butterworth–Heinemann; 2000.
[2] Gibson LJ, Ashby MF. Cellular Solids: structure and properties. second ed. Cambridge: Cambridge University Press; 1999.
[3] Delince M, Delannay F. Acta Mater 2004;52:1013.
[4] Markaki AE, Clyne TW. Acta Mater 2003;51:1341.
[5] Poquillon D, Viguier B, Andrieu E. EUROMECH, J Mater Sci, in press.
[6] Van Wyk CM. J Text Inst 1946;37:285.
[7] Toll S. Polym Eng Sci 1998;38:1337.
[8] Baudequin M, Ryschenkow G, Roux S. Eur Phys J B 1999;12:157.
[9] Rodney D, Fivel M, Dendievel R. Phys Rev Lett, in press.
[10] Markaki AE, Clyne TW. Acta Mater 2005;53:977.